Physiological Face Recognition Is Coming of Age

Pradeep Buddharaju Ioannis Pavlidis
Dept. of Computer Science, University of Houston
4800 Calhoun Rd, Houston, TX, 77004
braju@cs.uh.edu, ipavlidi@central.uh.edu
http://www.cpl.uh.edu

Abstract

The previous work of the authors has shown that physiological information on the face can be extracted from thermal infrared imagery and can be used as a biometric. Although, that work has proved the feasibility of physiological face recognition, the experimental results revealed high false acceptance rates due to methodological weaknesses in the feature extraction and matching algorithms. This paper, presents a new methodology that corrects these problems and yields high recognition rates. Specifically, a post-processing algorithm removes fake vascular contours, which degraded performance. Also, a new vascular network matching algorithm copes with deformations caused by varying facial pose and expressions. First, it estimates the facial pose in the test image and then calculates the deformation of the vascular network in the database image. Next, it registers test and database vascular networks using a dual bootstrap ICP matching algorithm. Finally, it computes a matching score between the vascular networks, which is a function of overlapping vessel pixels. Extensive experiments have been undertaken to test the new method. The results highlight its superiority.

1. Introduction

Face recognition stands as the most appealing biometric modality, since it is the natural mode of identification among humans and is totally unobtrusive. At the same time, however, it is one of the most challenging modalities [17]. Several face recognition algorithms have been developed in recent years mostly in the visible and a few in the infrared domain. A serious problem in visible face recognition is light variability, due to the reflective nature of incident light in this band. This clearly can be seen in Figure 1. The visible image of the same person in Figure 1(a) acquired in the presence of normal light appears totally different from that in Figure 1(b), which was acquired in low light.

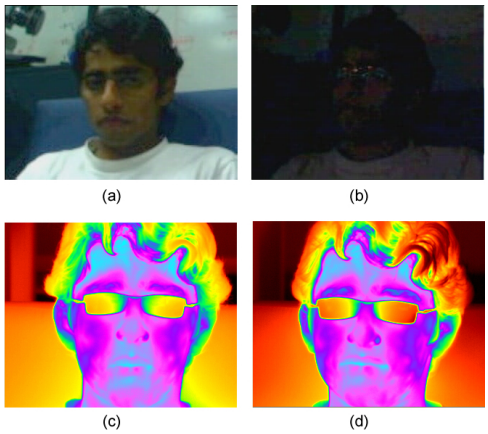

Figure 1. Example showing illumination effect on visible and thermal infrared images. All the images were acquired from the same subject at the same time. (a) Visible image in normal light. (b) Visible image in low light. (c) Thermal infrared image in normal light. (d) Thermal infrared image in low light.

Many of the research efforts in thermal face recognition were narrowly aiming to see in the dark or reduce the deleterious effect of light variability (Figure 1) [14, 11]. Methodologically, such approaches did not differ very much from face recognition algorithms in the visible band, which can be classified as appearance-based [7] and feature-based [4]. Recently, attempts have been made to fuse the visible and infrared modalities to increase the performance of face recognition [12, 16, 8, 10].

The authors have previously presented a physiological facial recognition method that promotes a different way of thinking about face recognition in thermal infrared [6, 3, 5]. This work has shown that facial physiological information, extracted in the form of superficial vascular network, can serve as good and time-invariant feature vector for face recognition. However, the methodology in that pilot work had some weak points. The recognition performance reported from the past experiments [6] can be substantially improved by curing these weaknesses. This paper

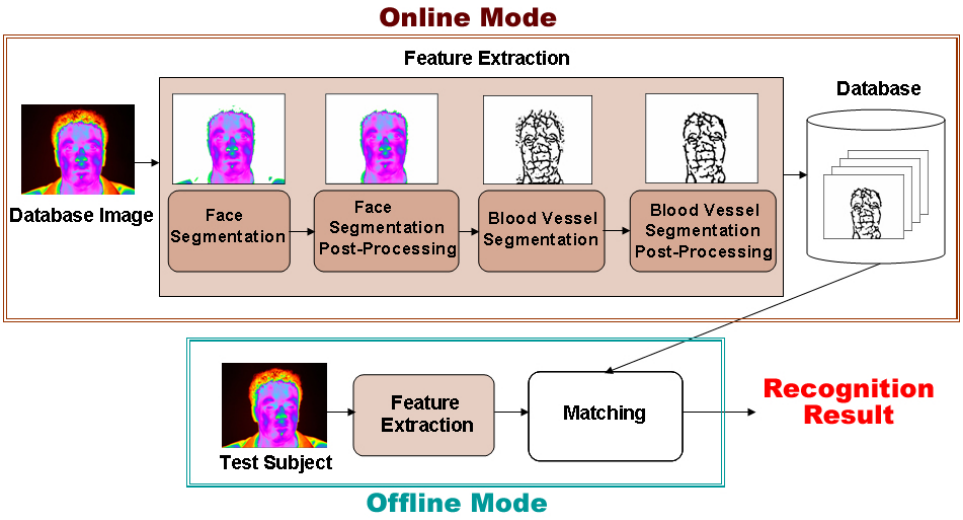

Figure 2. Methodological architecture.

presents an advanced methodological framework that aspires to transform physiological face recognition from feasible to viable. Specifically, the main contributions in the paper are:

- A new vessel segmentation post-processing algorithm that removes fake vascular contours detected by the top-hat vessel segmentation method
- A new vascular network matching algorithm that is robust to non-linear deformations due to facial pose and expression variations.
- Extensive comparative experiments to evaluate the performance of the new method with respect to previous methods.

The rest of the paper is organized as follows. Section 2 presents an overview of the new methodology. Section 3 presents in detail the vessel segmentation post-processing algorithm. Section 4 discusses the new vascular network matching algorithm. Section 5 presents the experimental results and attempts a critical evaluation. The paper concludes in Section 6.

2. Methodology

Figure 2 shows the methodological architecture. The method operates in the following two modes:

Off-line Mode: The thermal facial images are captured by a Mid-Wave Infrared (MWIR) camera. For each subject to be registered in the database, the feature extraction algorithm extracts the feature vector form the facial image and links it to the subject's record. The feature extraction algorithm has four steps:

First, a Bayesian ***face segmentation*** separates facial tissue from background. Second, ***face segmentation post-processing*** corrects face segmentation errors, which are due to occasional overlapping between portions of the tissue and background distributions. Third, a top-hat ***vessel segmentation*** algorithm extracts the vascular network from the facial segment after an anisotropic diffuser clarifies fuzzy edges, due to heat diffusion. These three steps have been adopted from [6]. Fourth, a new ***vessel segmentation post-processing*** algorithm, which is one of this paper's contriutions, corrects vessel segmentation. The vessel segmenter occasionally is fooled by areas of high contrast (e.g., hairline and skin edges) and reports them as vascular contours. These fake vascular contours participate in the matching process with deleterious effects.

On-line Mode: Given a query image, its vascular network is extracted using the feature extraction algorithm outlined in the off-line mode, and it is matched against vascular networks stored in the database. The new matching algorithm, which is another of this paper's contributions, has two stages:

First, a ***face pose estimation*** algorithm estimates the pose of the incoming test image, which is required to calculate the vascular network deformation between it and database images. Second, a ***dual bootstrap ICP matching*** algorithm registers the test and database vascular networks. The matching score between the two depends on the amount of overlapping.

3. Vessel Segmentation Post-Processing

A vessel's superficial thermal imprint is at a higher temperature than surrounding tissue due to convective heat produced from the flow of 'hot' arterial blood. The top-hat seg-

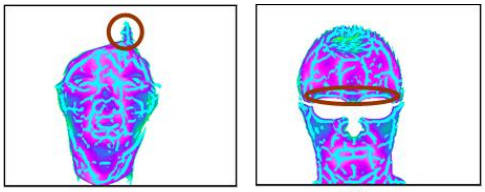

Figure 3. Errors from the top-hat segmentation algorithm for vasculature extraction: (a) Outliers due to facial hair; (b) Outliers due to glasses.

mentation algorithm is succesful in localizing vessels because it targets tansitions from hot to cold to hot. In some instances, such transitions are not due to the presence of vessels. Examples include tissue between hairlines or tissue between glasses and eyebrows (see Figure 3).

It is essential to detect and remove these outliers from the vascular network before applying a matching algorithm. To study in depth the properties of these outliers, the authors selected 25 representative subjects from the University of Houston dataset (kindly released for use) and analyzed the segmentation errors. Specifically, the authors identified the locations of both true vessels and outliers. Then, they drew measurement lines across each of the vessels and outliers and plotted the corresponding temperature profiles. They noticed that the variance between minimum and maximum temperature values was much larger in outliers than in true vessels. Indeed, the gradient in outliers is quite steep (several $^{\circ}C$), as it is formed between facial hair or glasses and tissue. By contrast, in true vessels, the gradient is quite small (only tenths of $^{\circ}C$), as it is formed between the projection of the vessel's lumen and surrounding tissue (Figure 4). Figure 5 shows the difference between minimum and maximum temperatures ($T_{max} - T_{min}$) across all the selected line profiles from the 25 representative subjects.

The new segmentation post-processing algorithm removes outliers based on the above findings. Specifically, it is carried out in the following steps:

Step 1: Skeletonize the vascular network to one pixel thickness;

Step 2: Draw a normal parallelogram across each skeleton pixel, and gather all the pixels covered by this parallelogram;

Step 3: Apply K-Means (with $K = 2$) on the pixels covered by this parallelogram. If the difference between the centers of each cluster is greater than 1.5, then mark it as an outlier pixel;

Step 4: Remove all the branches from the vascular network that have more than 50% of their pixels marked as outliers.

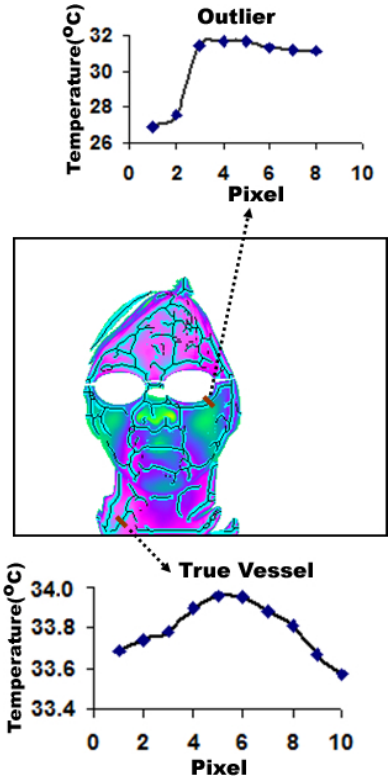

Figure 4. Temperature profiles of lines drawn across outliers and true vessels.

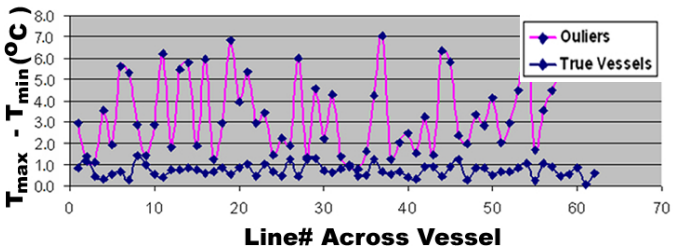

Figure 5. Difference between minimum and maximum temperatures for all the selected line profiles: (a) outliers; (b) true vessels.

After deleting the outliers from the vascular network, the remaining vascular map can be strored in the database.

4. Vascular Network Matching

The matching method presented in [6] could not cope with non-linearities in the deformation of the vascular network, due to variations in facial pose and expression. This paper presents a new vascular network matching algorithm that is robust to non-linear deformations.

4.1. Registration of Vascular Networks

The aim is to register the vascular network of the test image with that of the database image, so that they can be aligned. The iterative closest point (ICP) algorithm has ap-

pealing properties for point-based registration [2]. ICP requires proper initialization, as different instantiations of the ICP algorithm use different combinations of image points, distance metrics, and transformation models. In [15], Stewart *et al.* developed a variation of the ICP algorithm, called dual bootstrap ICP, that works well when initialization provides just a "toe hold" on the correct estimate of the transformation, and successfully registers elongated structures such as vasculature. Specifically, they reported good results on registration of retinal vascular images in the visible band. Since superficial vasculature extracted in thermal infrared has morphological resemblance to retinal vasculature in visible, the authors adopted the dual bootstrap algorithm for the registration task at hand.

After successful registration of the test and database vascular images, the matching score is computed based on the number of overlapping vessel pixels. If I_{test} represents the test vascular image with N_{test} vessel pixels, and I_{db} represents the database vascular image with N_{db} vessel pixels, the matching score is:

$$Score = \frac{N_{overlap}}{max(N_{test}, N_{db})} * 100, \qquad (1)$$

where $N_{overlap}$ represents the number of vessel pixels in I_{test} with a corresponding vessel pixel in I_{db} within a certain distance.

Figure 6 shows some examples of the performance of the dual bootstrap ICP algorithm in registering vascular images in thermal infrared. The example at the bottom row of the figure features substantial pose variation between the test and database images. The larger the pose variation the more difficult it becomes for the dual bootstrap ICP to cope successfully. This can be improved by estimating the pose of the test and database images, and setting the threshold value Thr accordingly. The pose estimation algorithm that was developed for this purpose, is presented in the next section.

4.2. Face Pose Estimation

At a neutral pose ($Pose = 0^o$) the nose is at center of the face, i.e., the position of the nose is halfway between the left and right ends of the face. From the face segmentation algorithm presented in [6], one can find the left and right ends of the face. Hence, if one localizes the nose, he/she can estimate the facial pose.

In a thermal infrared image, the nose is typically at a gradient with its surroundings, as shown in Figure 7. This is because of the tissue's shape (tubular cavity), its composition (artilage), and the forced circulation of air, due to breathing. The combinaion of all three, creates a nasal thermal signature which is different than that of the surrounding solid, soft tissue.

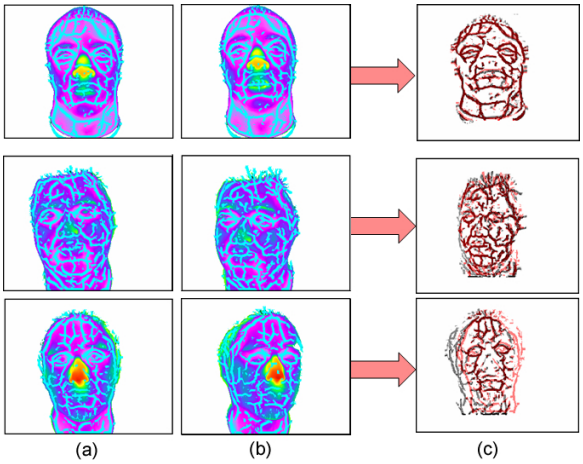

Figure 6. Registration performance examples: (a) Test vascular networks. (b) Database vascular networks. (c) Registration results.

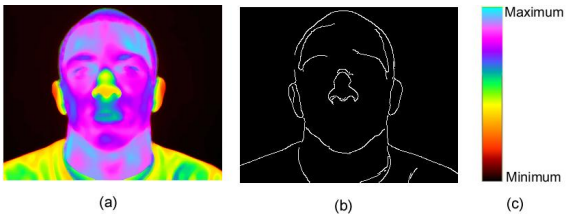

Figure 7. Nose edge extraction from thermal facial image: (a) thermal facial image; (b) edges extracted using canny edge detection algorithm; (c) color map

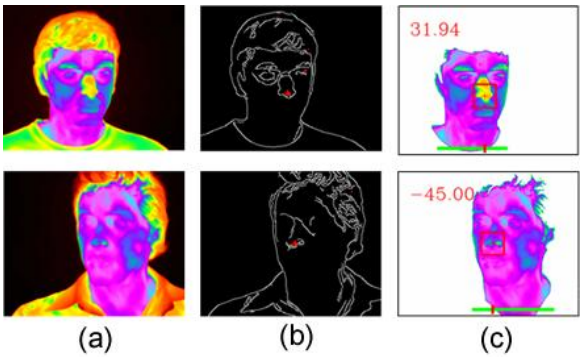

Figure 8. Pose estimation performance examples: (a) Thermal facial images. (b) Nose detection using Hausdorff-based matching. (c) Pose estimates.

By using a standard edge detection algorithm, one can extract the nose edges from the facial image. The next step is to search for the nose edge model in the facial edge map. The authors used a Hausdorff-based matching algorithm to localize the nose model in the face edge image [9]. Figure 8 shows some performance examples of the face pose estimation algorithm.

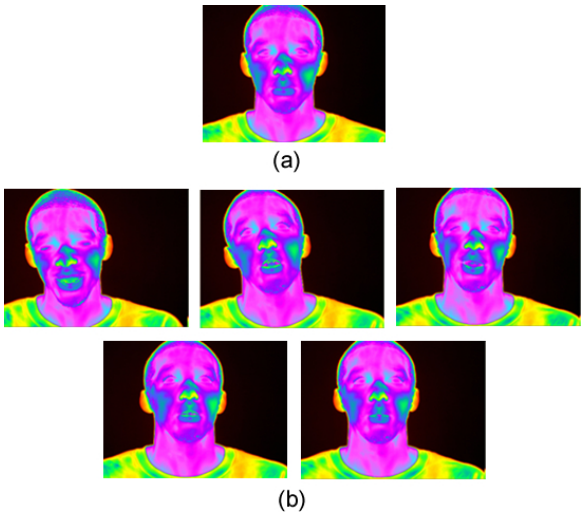

Figure 9. Sample subject from FEDS dataset: (a) One gallery image at neutral pose and expression; (b) Five probe images at varying facial expressions.

5. Experiments

The authors conducted several experiments to validate the performance of the new physiological face recognition method. This section presents the experimental setup and results in detail.

5.1. Experiments on the University of Houston Database

The authors have collected a huge thermal facial dataset at the University of Houston (UH) database for the purposes of this evaluation. This database has thermal facial images of varying expressions and poses from 300 subjects. The images were captured using a high quality Mid-Wave Infra-Red (MWIR) camera.

5.1.1 Facial Expression Dataset (FEDS)

To test the performance of the new method in the presence of varying facial expressions between gallery and probe images, the authors created the facial expression dataset (FEDS) out of the UH database as follows: From each of the 300 subjects one frontal facial image at 0^o pose and neutral expression was used as a gallery image. Then, five different facial images at 0^o pose but with varying facial expressions were used as probe images for each subject. Hence, FEDS has a total of 300 gallery images and 1500 probe images from 300 subjects. Figure 9 shows a sample subject set from FEDS.

Figures 10(a) and 10(b) show respectively the CMC and ROC curves of the FEDS experiments using the TMP matching algorithm reported in [6] versus the dual bootstrap ICP matching algorithm.

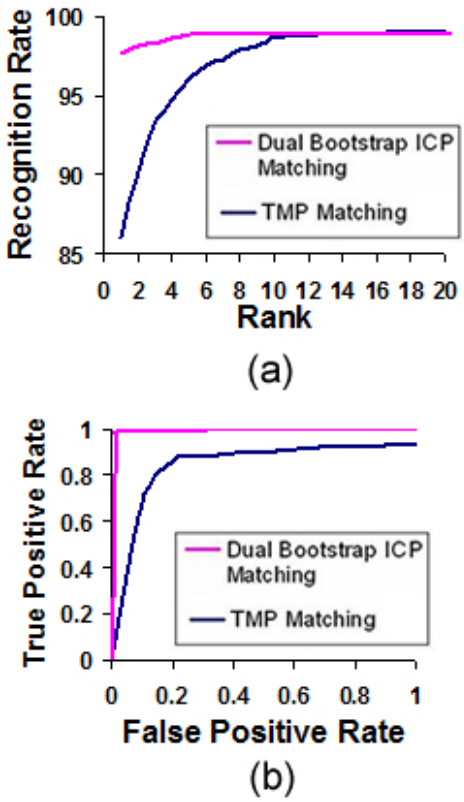

Figure 10. Experimental results on the FEDS dataset using dual bootstrap ICP versus TMP matching: (a) CMC curves. (b) ROC Curves.

The results demonstrate that the dual bootstrap ICP matching outperforms the TMP matching algorithm. In the case of TMP matching, the CMC curve shows that rank 1 recognition is 86%, whereas for the for dual bootstrap ICP is 97%. Also, the dual bootstrap ICP matching method achieves a high positive detection rate at very low false detection rates, as shown in Figure 10(b). This indicates that the ICP matching algorithm is highly robust to deformations caused in the vascular network by facial expression variations.

5.1.2 Facial Pose Dataset (FPDS)

To test the performance of the new method in the presence of varying poses between gallery and probe images, the authors created the facial pose dataset (FPDS) out of the UH database as follows: From each of the 300 subjects one frontal facial image at 0^o pose and neutral expression was used as a gallery image. Then, four different facial images at neutral facial expression, but at varying poses between -30^o and 30^o were used as probe images. Hence, FPDS has a total of 300 gallery images and 1200 probe images from 300 subjects. Figure 11 shows a sample subject set

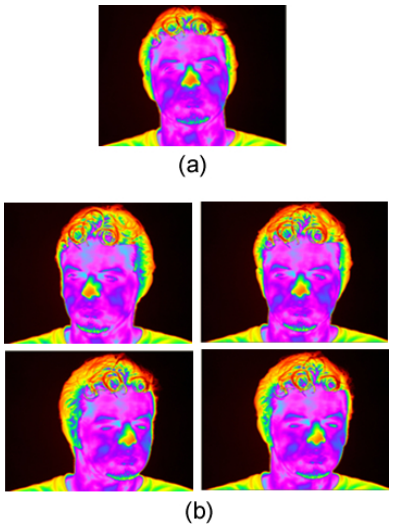

Figure 11. Sample subject from FPDS dataset: (a) One gallery image at neutral pose and expression. (b) Four probe images at varying poses.

from FPDS.

Figures 12(a) and 12(b)show the results of the FPDS experiments using the dual bootstrap ICP matching algorithm. The results demonstrate that the algorithm copes well with facial pose variations between gallery and probe images. Specifically, the CMC curve shows that rank 1 recognition is 89%, and the ROC curve shows that it requires a false acceptance rate over 5% to reach a positive acceptance rate above the 90% range. One can notice that the false acceptance rate on FPDS experiments is a bit higher than on FEDS experiments. This is to be expected, as variations in pose typically cause more non-linear deformations in the vascular network than those caused by variations in facial expressions.

5.2. Experiments on the University of Notre Dame's Database

A major challenge associated with thermal face recognition is the recognition performance over time [13]. Facial thermograms may change depending on the physical condition of the subject making it difficult to acquire similar features for the same person over time. Previous face recognition methods in thermal infrared that used raw thermal data reported degraded performance over time [7, 8]. Facial physiological information, however, remains invariant to physical conditions because the thermal contrast between the vascular and surrounding pixels is maintained (natural constant).

Since most of the subjects in the UH database had images collected during the same session, no statistically significant quantification of the low permanence problem was possible. For this reason, the authors obtained clearance to

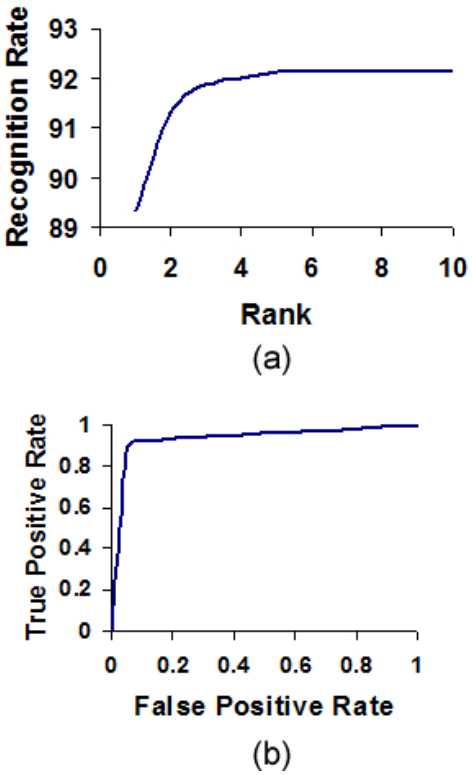

Figure 12. Experimental results on the FPDS dataset using the dual bootstrap ICP matching algorithm: (a) CMC curve. (b) ROC Curve.

apply the method on another data set, that of the University of Notre Dame (UND) [1]. This database has a large collection of visible and thermal facial images acquired with a time-gap. The database consists of 2294 images acquired from 63 subjects during 9 different sessions under specific lighting (LF - central light turned off, LM - all three lights on) and facial expression conditions (FA - neutral expression, FB - smiling expression).

The database is divided into four different gallery and probe sets [7]: LF + FA, LF + FB, LM + FA, LM + FB. Each of the gallery sets (say LF—FA) can be tested against the other three probe sets (say LF—FB, LM—FA, and LM—FB). Thus, 12 different pairs of gallery and probe sets were used for testing. The performance of the new dual-bootstrap ICP matching algorithm was compared to that of TMP matching [6], and PCA matching [7] algorithms. Table 1 summarizes the rank 1 recognition results of these algorithms on each of the 12 experiments. Each entry in the left column of the table corresponds to a gallery set, and each entry in the top row corresponds to a probe set. From the table, it can be clearly seen that the new matching algorithm yields better recognition results even in the presence of time and temperature variations, thus, outperforming the TMP (legacy physiology-based) and PCA (legacy raw thermal-based) recognition algorithms.

Gallery	Probe			
	FA—LF	FA—LM	FB—LF	FB—LM
FA—LF	-	86.54% (DBICP)	84.38% (DBICP)	83.33% (DBICP)
	-	82.65% (TMP)	80.77% (TMP)	81.33% (TMP)
	-	78.74% (PCA)	76.83% (PCA)	75.77% (PCA)
FA—LM	83.65% (DBICP)	-	84.24% (DBICP)	82.45% (DBICP)
	81.46% (TMP)	-	79.38% (TMP)	80.25% (TMP)
	79.23% (PCA)	-	75.22% (PCA)	73.56% (PCA)
FB—LF	85.48% (DBICP)	88.87% (DBICP)	-	85.82% (DBICP)
	80.27% (TMP)	81.92% (TMP)	-	80.56% (TMP)
	74.88% (PCA)	76.57% (PCA)	-	74.23% (PCA)
FB—LM	83.39% (DBICP)	87.34% (DBICP)	85.56% (DBICP)	-
	80.67% (TMP)	82.25% (TMP)	79.46% (TMP)	-
	69.56% (PCA)	74.58% (PCA)	78.33% (PCA)	-

Table 1. Rank1 recognition performance of Dual Bootstrap Iterative Closest Point (DBICP) vascular network matching algorithm, Thermal Minutia Point (TMP) matching algorithm [6], and PCA algorithm [8] on each of the 12 experiments on the UND database.

5.3. Experiments on the University of Arizona's Database

The authors have also acquired permission to use data from a stress experiment carried out by the University of Arizona (UA). These data, although acquired within a few minutes for each subject, feature dramatic changes in the facial thermal map due to the onset of stress. In fact, in a few minutes a lot more variability is present than the one in UND, which took months to assemble. The length of each experiment is approximately 20 minutes. For each subject, the authors extracted around five, equally time-spaced frames from the interview. One sample subject from the database is shown in Figure 13. It can clearly be seen from the visualization on forehead and neck that the thermal map changed significantly between database (Figure 13(a)) and test images (Figure 13(b)).

Figure 14(a) shows the the Cumulative Math Characteristic (CMC) curves and Figure 14(b) shows the ROC curves of the UA experiments using the dual bootstrap ICP matching versus the TMP matching algorithms. The results demonstrate that the dual bootstrap ICP matching algorithm again outperforms the TMP matching algorithm [6]. In the case of TMP matching, the CMC curve shows that rank 1 recognition is 83.6% whereas for ICP is 93.2%. Also, the dual bootstrap ICP matching method achieves a high positive detection rate at very low false detection rates, as it is shown in Figure 14(b).

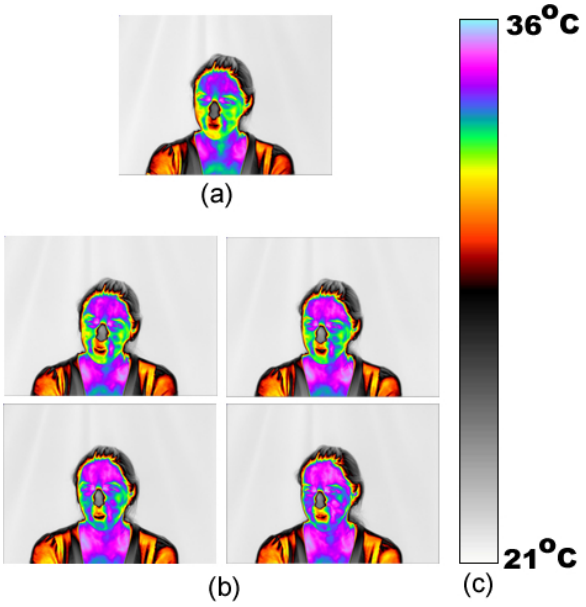

Figure 13. Sample subject from UA dataset: (a) One database image extracted at 2 minutes 6 seconds of the interview; (b) Four test images extracted at 6 minutes, 9 minutes 18 seconds, 13 minutes 22 seconds, and 17 minutes 40 seconds of the interview respectively. (c) Thermal color map used for visualization.

6. Conclusions

This paper presents new algorithms that substantially improve the performance of physiology-based face recognition in the thermal infrared. Specifically, a vascular network post-processing algorithm removes fake contours detected by vessel segmentation algorithm. A new vascular network matching algorithm can cope with non-linear deformations between test and database vascular networks.

The experimental results on UH, UND, and UA databases, which are non-trivial sets, confirm the superiority of the new method.

Acknowledgments

The authors would like to thank the University of Notre Dame for kindly providing IR images acquired during different sessions, and also the University of Arizona for con-

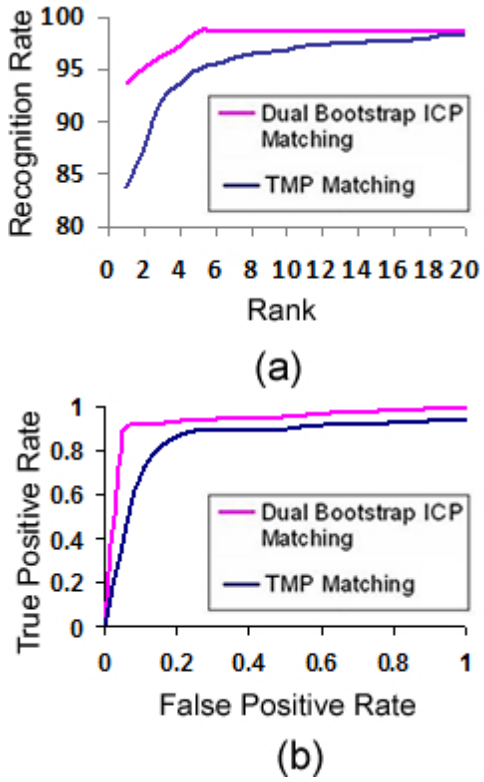

Figure 14. Results of the experiments on the UA database using dual bootstrap ICP matching versus TMP matching: (a) CMC curves. (b) ROC Curves.

ducting the stress experiments. This research was supported mainly by NSF grant # DUE-0313880 in "Collaborative Research: Capacity Expansion in Information Assurance" and NSF grant # IIS-0414754 in "Interacting with Human Physiology". The views expressed in this paper do not necessarily represent the views of the funding Agencies.

References

[1] T. C. V. L. at the University of Notre Dame. Biometrics database distribution. http://www.nd.edu/ cvrl/. 6

[2] P. Besl and N. McKay. A method for registration of 3-d shapes. *IEEE Transactions on Pattern Analysis and Machine Intelligence*, 14(2):239–256, 1992. 4

[3] P. Buddharaju and I. Pavlidis. *Advances in Biometrics: Sensors, Systems and Algorithms*, chapter Face Recognition Beyond the Visible Spectrum. Springer, in print. 1

[4] P. Buddharaju, I. Pavlidis, and I. Kakadiaris. Face recognition in the thermal infrared spectrum. In *Proceedings of the Joint IEEE Workshop on Object Tracking and Classification Beyond the Visible Spectrum*, Washington D.C., June 2004. 1

[5] P. Buddharaju, I. Pavlidis, and P. Tsiamyrtzis. Pose-invariant physiological face recognition in the thermal infrared spectrum. In *Proceedings of the 2006 IEEE Conference on Computer Vision and Pattern Recognition*, pages 53–60, New York, New York, June 17 2006. 1

[6] P. Buddharaju, I. Pavlidis, P. Tsiamyrtzis, and M. Bazakos. Physiology-based face recognition in the thermal infrared spectrum. *IEEE Transactions on Pattern Analysis and Machine Intelligence*, 29(4):613–626, April 2007. 1, 2, 3, 4, 5, 6, 7

[7] X. Chen, P. Flynn, and K. Bowyer. PCA-based face recognition in infrared imagery: Baseline and comparative studies. In *Proceedings of the IEEE International Workshop on Analysis and Modeling of Faces and Gestures*, pages 127–134, Nice, France, October 17 2003. 1, 6

[8] X. Chen, P. Flynn, and K. Bowyer. Ir and visible light face recognition. *Computer Vision and Image Understanding*, 99(3):332–358, September 2005. 1, 6, 7

[9] D. P. Huttenlocher, G. A. Klanderman, and W. A. Rucklidge. Comparing images using the hausdorff distance. *IEEE Transactions on Pattern Analysis and Machine Intelligence*, 15(9):850–863, 1993. 4

[10] S. G. Kong, J. H. anf B. R. Abidi, J. Paik, and M. A. Abidi. Recent advances in visual and infrared face recognition-a review. *Computer Vision and Image Understanding*, 97(1):103–135, January 2005. 1

[11] A. Selinger and D. Socolinsky. Face recognition in the dark. In *Proceedings of the Joint IEEE Workshop on Object Tracking and Classification Beyond the Visible Spectrum*, Washington D.C., June 2004. 1

[12] D. Socolinsky and A. Selinger. Thermal face recognition in an operational scenario. In *Proceedings of the IEEE Computer Society Conference on Computer Vision and Pattern Recognition*, volume 2, pages 1012–1019, Washington, D.C, June 2004. 1

[13] D. Socolinsky and A. Selinger. Thermal face recognition over time. In *Proceedings of the 17th International Conference on Pattern Recognition*, volume 4, pages 23–26, August 2004. 6

[14] D. Socolinsky, L. Wolff, J. Neuheisel, and C. Eveland. Illumination invariant face recognition using thermal infrared imagery. In *Proceedings of the IEEE Computer Society Conference on Computer Vision and Pattern Recognition(CVPR 2001)*, volume 1, pages 527–534, Kauai, Hawaii, United States, 2001. 1

[15] C. V. Stewart, C. Tsai, and B. Roysam. The dual-bootstrap iterative closest point algorithm with application to retinal image registration. *IEEE Transactions on Medical Imaging*, 22(11):1379–1394, 2003. 4

[16] J.-G. Wang, E. Sung, and R. Venkateswarlu. Registration of infrared and visible-spectrum imagery for face recognition. In *Proceedings of the Sixth IEEE International Conference on Automatic Face and Gesture Recognition*, pages 638–644, Seoul, Korea, May 2004. 1

[17] W. Zhao, R. Chellappa, P. J. Phillips, and A. Rosenfeld. Face recognition: A literature survey. *ACM Computing Surveys (CSUR)*, 35(4):399–458, December 2003. 1